# Extended depth-of-focus by digital holographic microscopy

**Tristan Colomb,[1,*] Nicolas Pavillon,[2] Jonas Kühn,[2] Etienne Cuche,[1] Christian Depeursinge,[2] and Yves Emery[1]**

[1]*Lyncée Tec SA, PSE-A, CH-1015 Lausanne, Switzerland*

[2]*Laboratoire d'Optique Appliquée, Ecole Polytechnique Fédérale de Lausanne, CH-1015 Lausanne, Switzerland*

**Corresponding author: tristan.colomb@lynceetec.com*

Received March 12, 2010; accepted April 16, 2010;
posted April 28, 2010 (Doc. ID 125425); published May 24, 2010

A recurrent problem in microscopy is the finite depth-of-focus linked to the NA of microscope objectives. Digital holographic microscopy (DHM) has the unique feature of being able to numerically change the focus from a single hologram without the need of moving the sample. Extended depth of focus of amplitude images has been demonstrated, but it has marginal interest for the metrological application of DHM that needs the topography. In this Letter, we demonstrate that DHM is able to provide not only extended depth-of-focus amplitude images but extended focused complex data from which the topography is computed. For this purpose, reflection and transmission measurements on micro-optics (microlens and retroreflector) performed by using standard reconstruction or the extended focused complex data are compared. These experiments demonstrate that DHM measures, from a single hologram acquisition, the accurate sample topography on a numerically increased depth-of-focus. 

*OCIS codes:* 090.1995, 180.3170, 100.2980.

Digital holographic microscopy (DHM) allows the measurement of the complex wavefront reflected by, or transmitted through, an object. From the quantitative phase measurement, the topography of the object is computed [1]. As the phase is defined modulo $2\pi$, DHM optical path length measurement without phase ambiguity is commonly limited to the range of the wavelength (transmission) or half the wavelength (reflection). By use of unwrapping procedures or multiple wavelengths that synthesize a larger wavelength up to several micrometers [2,3], DMH can investigate objects much higher than the microscope objective (MO) depth of field (DOF). For this reason, as in bright-field microscopy, the areas outside the DOF give out-of-focus and blurred amplitude. Using the unique numerical focusing capability of DHM, Ferraro *et al.* demonstrated in [4] extended focused amplitude imaging. Nevertheless, as metrology is the main application of DHM, the error introduced by the limited depth-of-focus on the quantitative phase image is much more important to suppress. Therefore, an extended depth of focus (EDOF) of the complex image (amplitude and phase) is of a larger interest. To our knowledge, this Letter presents for the first time a method to reconstruct EDOF complex images for reflection and transmission DHM. The principle is validated by an example in reflection, for which microlens profiles achieved with EDOF DHM and atomic force microscopy (AFM) are compared, and in transmission by measuring a high-aspect-ratio retroreflector.

The digital holographic microscope records a hologram, resulting from the off-axis interference between a reference wave and an object wave $\Psi$ reflected by, or transmitted through, a specimen, and magnified by an MO (Fig. 1). Even if it is possible to record a digital hologram of the sharply focused object in the plane of the CCD sensor [5], most of the time the MO does not form the specimen image on the detector but behind or in front of the CCD camera. From a single hologram, the numerical wavefront in the hologram plane is reconstructed. Then, this wavefront is propagated numerically along the optical axis to the image plane, defined by the numerical distance $d$, according to the convolution formalism [6]. The reconstructed complex wavefront $\Psi_d = A_d(x,y)\exp[i\phi_d(x,y)]$ provides the amplitude image $A_d$ and the phase image $\phi_d$.

From the reconstructed phase $\phi_d$, the topography $H_c$ of the specimen is computed for the reflection ($c = r$) or transmission ($c = t$) configurations:

$$H_r(x,y) = \phi_d\lambda/(4\pi n_m), \tag{1}$$

$$H_t(x,y) = \phi_d\lambda/[2\pi(n_s - n_m)], \tag{2}$$

where $\lambda$ is the wavelength of the source and $n_m$ and $n_s$ are the refractive indices of the medium (usually air) and the specimen, respectively.

Figure 1 presents the DHM optical schematic. The depth of focus (width of the right rectangle) is related to the DOF (width of the left rectangle) defined by the relation

$$\mathrm{DOF} = \lambda n_m/\mathrm{NA}^2, \tag{3}$$

where NA is the numerical aperture of the MO. The reconstructed wavefront, obtained for the reconstruction distance $d_0$, is therefore in focus for the areas inside the

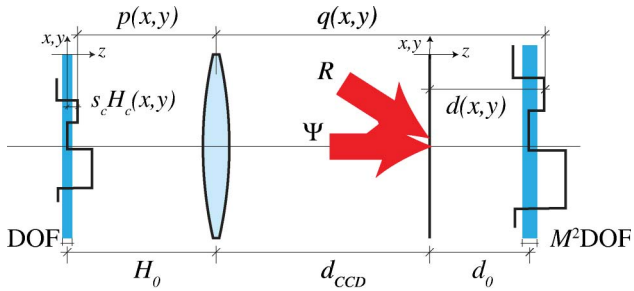


Fig. 1. (Color online) DHM optical schematic: $M$, magnification.

 

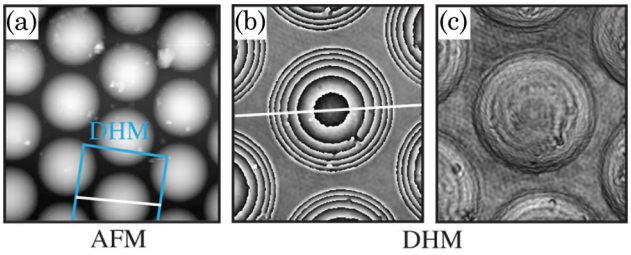


Fig. 2. (Color online) Microlens array imaged by (a) AFM and (b), (c) DHM in (b) phase and (c) amplitude contrasts with a 50× MO (NA = 0.75) and with a wavelength of $\lambda = 682.5$ nm.

DOF and out of focus elsewhere. Figures 2(b) and 2(c) present the amplitude and phase images obtained in reflection configuration for a microlens measured in air ($n_m = 1$) with $\lambda = 682.5$ nm, and a 50× MO with NA = 0.75. The reconstruction distance $d_0$ is adjusted to focus the microlens edges. Because the microlens is higher than the DOF = 1.2 $\mu$m, one notes clearly that dust particles on the top of the amplitude image are not focused [Fig. 2(b)]. The same blurring effect appears on the phase image and distorts the measured shape of the lens, as shown in Fig. 3. The comparison between the DHM height profile [along white line on Fig. 2(b)], computed from Eq. (2) after phase unwrapping, and the height profile measured with the AFM (Veeco AFM Explorer) along the white line on Fig. 2(a), demonstrates clearly in the inset of Fig. 3 the deformation introduced by the finite DOF.

In order to retrieve the correct shape, the EDOF complex wavefront has to be computed by using different reconstruction distances $d(x,y)$ for each pixel $(x,y)$. From the magnification definition $M = -q/p$, the thin lens equation $1/f = 1/p + 1/q$ [$f$, the MO focal length, $p(x,y) = H_0 + s_c H_c(x,y)$, $q(x,y) = d_{\mathrm{CCD}} + d(x,y)$ defined in Fig. 1, $s_r = +1$ in reflection and $s_t = -1$ in transmission], one deduces the relation [4]

$$d(x,y) = -s_c M^2 H_c(x,y) + d_0. \tag{4}$$

From the initial topography $H_c(x,y)$, achieved with a 2D unwrapped phase [Fig. 4(a)] (or from dual-wavelength method when unwrapping procedures in reflection are not possible [3]), the reconstruction distance map $d(x,y)$ can be reconstructed from Eq. (4) and allows the reconstruction of the EDOF complex wavefront: $\Psi_{\mathrm{EDOF}}(x,y) = \Psi_{d(x,y)}(x,y)$.

To reduce the computation time, the distance map is sampled from $d_{\min}$ to $d_{\max}$ with a sampling step $\delta d$ that is computed according to Eq. (4) by using the initial

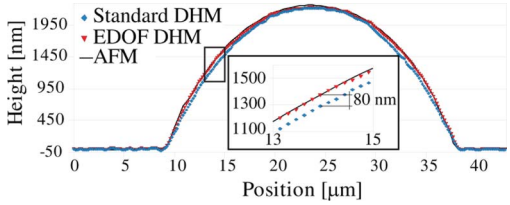


Fig. 3. (Color online) Comparison between profiles measured along the white lines defined on Figs. 2(a), 2(b), and 4(b), corresponding to AFM, standard DHM, and EDOF DHM images. The detail shows clearly that EDOF gives the right profile.

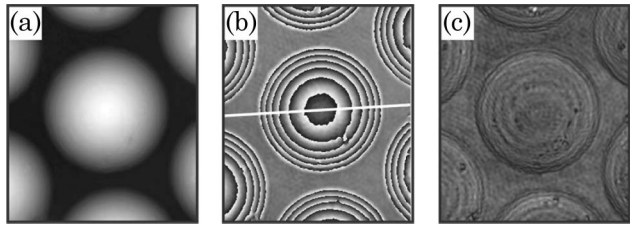


Fig. 4. (a) 2D unwrapped image of Fig. 2(b); (b) phase and (c) amplitude EDOF images obtained from the topography (a).

topography $H_c(x,y)$, extrema $H_{c,\min}$ and $H_{c,\max}$, and the height sampling step $\delta H$ defined from DOF as

$$\delta H = \mathrm{DOF}/P, \tag{5}$$

where $P \geq 1$. To preserve a good continuity, the presented results are achieved with $P = 3$. The EDOF method consists now on numerically scanning with $N$ steps $[N = (H_{c,\max} - H_{c,\min})/\delta H]$ the reconstruction distances $d_n = d_{\min} + n\delta d$ $(n = 0, N-1)$ and to fill $\Psi_{\mathrm{EDOF}}(i,j)$ with the values of $\Psi_{d_n}(i,j)$ when $d_n \leq d(i,j) < d_{n-1}$.

Figures 4(c) and 4(d) respectively present the EDOF amplitude and phase images achieved with $M = 50$, NA = 0.75, $\lambda = 682.5$ nm, and $n_m = 1$. All the dust particles are clearly focused, and the height profile (Fig. 3) matches the AFM measurement in very good agreement. The initial DOF = 1.2 $\mu$m is increased numerically by about a factor of 2, as the height of the microlens is about 2.3 $\mu$m.

Figure 5 presents the amplitude and phase reconstructions obtained for a high-aspect-ratio retroreflector ($n_s = 1.52$), immersed in distilled water ($n_m = 1.332$), measured in transmission at $\lambda = 664$ nm with a ×60 MO (NA = 1.3) giving a DOF = 0.52 $\mu$m, and computed with different reconstruction distances. The EDOF complex wavefront is computed by adjusting the reconstruction distance $d_0 = 3.6$ cm to focus the retroreflector edges [Fig. 5(a)]. The EDOF complex wavefront reconstruction gives the amplitude and phase images presented in Fig. 5(d). The phase profiles along the white lines are unwrapped to provide height profiles using Eq. (2) (Fig. 6). EDOF topography gives straight-face slopes as expected, contrary to single reconstruction-distance measurements, and demonstrates a numerical increase of the DOF to 20 $\mu$m (increase of a factor of

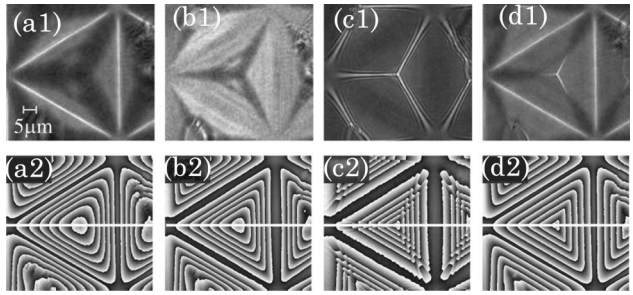


Fig. 5. Amplitude (1) and phase (2) reconstructions of a high-aspect-ratio retroreflector ($n_s = 1.52$) immersed in distilled water ($n_m = 1.332$) measured in transmission with a 60× MO, NA = 1.3 for different reconstruction distances (a) 3.6 cm, (b) 6.6 cm, (c) 11.0 cm, and (d) with the presented EDOF method.

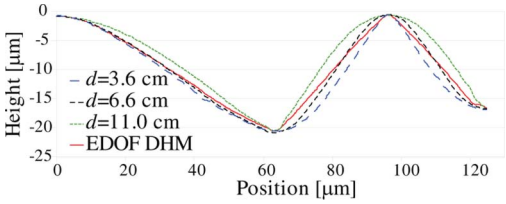


Fig. 6. (Color online) Height profile computed from the phase measured along white lines defined in Fig. 5 for different reconstruction distances and for EDOF DHM.

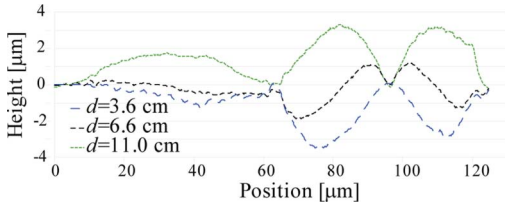


Fig. 7. (Color online) Difference between the reconstruction distances and the EDOF profiles.

40). Figure 7 shows the difference between the different reconstruction-distance profiles and the EDOF height profile. The standard deviation for each reconstruction distance 3.6 cm, 6.6 cm, and 11.04 cm is, respectively, 1.04 $\mu$m, 0.68 $\mu$m, and 0.99 $\mu$m. It demonstrates that the height measurement error is not negligible when a single reconstruction distance is used.

One should note that, theoretically, this technique could increase numerically the DOF to infinity, but there are practically physical limitations as the MO working distance and the source coherence: surface parts of the object too far from the MO pupil are poorly imaged by the MO or are out of coherence (no DHM signal). Second, the EDOF complex wavefront is computed from an initial height that has some deformation and height error. An iterative procedure that takes the EDOF results to define the initial height could be done to improve the accuracy of the topographic reconstruction. Finally, a complete automation of this procedure should be possible using an autofocus algorithm to adjust the reconstruction distance $d_0$ [7].

We have demonstrated that DHM allows extended focused complex wavefronts obtained in reflection or transmission DHM configurations. It allows to reconstruct not only the extended focused amplitude images but especially the real topography for object higher than the DOF of the microscope objective. A numerical increase of the DOF up to 40 times in the case of a high-aspect-ratio retroreflector measured in transmission with a 60× MO is demonstrated.

The authors thank Bamdad Afra from the Laboratoire d'optique appliquée in the Ecole Polytechnique Fédérale de Lausanne for the delivery of the AFM measurements. The research leading to these results has received funding from the European Community's Seventh Framework Programme FP7/2007-2013 under grant agreement no. 216105.

**References**

1. E. Cuche, P. Marquet, and C. Depeursinge, Appl. Opt. **38**, 6994 (1999).
2. J. Gass, A. Dakoff, and M. Kim, Opt. Lett. **28**, 1141 (2003).
3. J. Kühn, T. Colomb, F. Montfort, F. Charrière, Y. Emery, E. Cuche, P. Marquet, and C. Depeursinge, Opt. Express **15**, 7231 (2007).
4. P. Ferraro, S. Grilli, D. Alfieri, S. Nicola, A. Finizio, G. Pierattini, B. Javidi, G. Coppola, and V. Striano, Opt. Express **13**, 6738 (2005).
5. B. Kemper, D. Carl, J. Schnekenburger, I. Bredebusch, M. Schäfer, W. Domschke, and G. von Bally, J. Biomed. Opt. **11**, 034005 (2006).
6. T. Colomb, F. Montfort, J. Kühn, N. Aspert, E. Cuche, A. Marian, F. Charrière, S. Bourquin, P. Marquet, and C. Depeursinge, J. Opt. Soc. Am. A **23**, 3177 (2006).
7. P. Langehanenberg, B. Kemper, D. Dirksen, and G. von Bally, Appl. Opt. **47**, D176 (2008).